Topology optimization of hyperelastic bodies including non-zero prescribed displacements

Anders Klarbring and Niclas Strömberg

Topology Optimization of Hyperelastic Bodies including Non-Zero Prescribed Displacements

Anders Klarbring[†] and Niclas Strömberg[*]

[†]Mechanics
Department of Management and Engineering
The Institute of Technology
Linköping University
SE-581 83 Linköping, Sweden
E-mail: anders.klarbring@liu.se

[*]Department of Mechanical Engineering
Jönköping University
SE-551 11 Jönköping, Sweden
E-mail: niclas.stromberg@jth.hj.se

February 4, 2013

Abstract

Stiffness topology optimization is usually based on a state problem of linear elasticity, and there seems to be little discussion on what is the limit for such a small rotation-displacement assumption. We show that even for gross rotations that are in all practical aspects small ($< 3\,\mathrm{deg}$), topology optimization based on a large deformation theory might generate different design concepts compared to what is obtained when small displacement linear elasticity is used. Furthermore, in large rotations, the choice of stiffness objective (potential energy or compliance), can be crucial for the optimal design concept. The paper considers topology optimization of hyperelastic bodies subjected simultaneously to external forces and prescribed non-zero displacements. In that respect it generalizes a recent contribution of ours to large

deformations, but we note that the objectives of potential energy and compliance are no longer equivalent in the non-linear case. We use seven different hyperelastic strain energy functions and find that the numerical performance of the Kirchhoff-St.Venant model is in general significantly worse than the performance of the other six models, which are all modifications of this classical law that are equivalent in the limit of infinitesimal strains, but do not contain the well-known collapse in compression. Numerical results are presented for two different problem settings.

Keywords: Hyperelasticity, Potential energy, Compliance, Optimality criteria

1 Introduction

The majority of works on topology optimization of structures concerns linear elastic bodies, and stiffness optimization is performed for a situation where prescribed displacements are set to zero. Topology optimization studies of linear elastic bodies subjected to both external forces and prescribed non-zero displacements are more rare. Recently, however, this was studied by optimizing (minimizing/maximizing) the compliance in Niu et al. [1] and a discussion on the topic was also contributed by Pedersen and Pedersen [2]. Moreover, in a recent publication [3], we show how maximizing potential energy is the natural objective in stiffness optimization of structures and unifies the situation of simultaneously applied external forces and non-zero displacements. In the present paper we deal with large displacement problems, where the situation of non-zero prescribed displacements is even more important than in the small displacement case. We are concerned with comparing objectives of potential energy and compliance, and therefore of didactic reasons we begin this introduction by a short discussion of the small displacement case.

Consider a discrete linear elastic body subjected to external forces $\boldsymbol{F}$ and a prescribed displacement δ, which can be related to a vector of nodal displacements $\boldsymbol{d}$ such that, for a prescribed column vector $\boldsymbol{e}$, $\boldsymbol{e}^T\boldsymbol{d} = \delta$. The state of equilibrium is obtained by minimizing the potential energy

$$\Pi(\boldsymbol{\rho}, \boldsymbol{d}) = \frac{1}{2}\boldsymbol{d}^T\boldsymbol{K}(\boldsymbol{\rho})\boldsymbol{d} - \boldsymbol{F}^T\boldsymbol{d}$$

with respect to the admissible displacements. Here, $\boldsymbol{K}(\boldsymbol{\rho})$ is a stiffness matrix that depends on design variables $\boldsymbol{\rho}$. The optimality condition

associated with this minimization problem is

$$\boldsymbol{K}(\boldsymbol{\rho})\boldsymbol{d} = \boldsymbol{F} + \lambda \boldsymbol{e}. \tag{1}$$

In this state equation, the Lagrange multiplier λ can be interpreted as the reaction force needed to satisfy the kinematic constraint $\boldsymbol{e}^T\boldsymbol{d} = \delta$. Solving the optimality condition (1) together with the kinematic constraint gives $\boldsymbol{d} = \boldsymbol{d}(\boldsymbol{\rho})$ and $\lambda = \lambda(\boldsymbol{\rho})$. As an objective function in stiffness optimization we now take the equilibrium potential energy $\Pi(\boldsymbol{\rho}, \boldsymbol{d}(\boldsymbol{\rho}))$ and maximize this with respect to the design. It is also shown, by using (1), that

$$\Pi(\boldsymbol{\rho}, \boldsymbol{d}(\boldsymbol{\rho})) = -\frac{1}{2}\boldsymbol{F}^T\boldsymbol{d}(\boldsymbol{\rho}) + \frac{1}{2}\lambda(\boldsymbol{\rho})\delta. \tag{2}$$

Thus, maximizing the potential energy is equivalent to simultaneously minimizing the compliance of the external forces and maximizing the compliance of the prescribed displacement. If only the external forces are included, then this is also equivalent to minimizing the elastic energy. On the contrary, when only the prescribed displacement is included, then maximizing the elastic energy is equivalent to (2). However, in the general case involving both external forces and the non-zero prescribed displacement, (2) means neither maximizing nor minimizing the elastic energy. Now, for a hyperelastic body undergoing large displacements, the equivalences given in (2) does not hold. Furthermore, the compliance problem, i.e. the right hand side of (2), does not have the familiar property that no adjoint equation is needed to calculate sensitivities, while this is still true for the problem of maximizing the potential energy. In this work, these two objectives are compared and studied for non-linear hyperelastic bodies and the performance of seven different hyperelastic strain energy potentials is investigated.

Buhl et al. [4] is an early work on topology optimization of structures formulated in a setting of large displacements. They used a total Lagrangian formulation and coupled the Green-Lagrange strain and the second Piola-Kirchhoff stress via the Kirchhoff-St.Venant law of elasticity. Different objectives were studied by adjoint sensitivity analysis. Similar works were presented by Gea and Luo [5], and Bruns and Tortelli [6]. In the latter work compliant mechanisms were also studied by using the Kirchhoff-St.Venant model. Topology synthesis of large displacement compliant mechanisms were at the same time investigated by Pedersen et al. [7]. Jung and Gea [8] considered non-linear structures by coupling the effective strain to the effective stress by using a power law. Bruns et al. [9] solved topology optimization problems of structures that exhibit snap-through by using an arc-length method. This work

was extended by Bruns and Sigmund [10] to also incorporate mechanisms. Large deformations and stability in topology optimizations were also investigated by Kemmler et al. [11]. Instead of using a total Lagrangian formulation, Pajot and Maute [12] used a co-rotational formulation for studying topology optimization of non-linear structures. An example of an applied work is Lee and Youn [13], who optimized rubbber isolaters by using the Mooney-Rivlin model.

In this work a total Lagrangian formulation is adopted. The Green-Lagrange strain and the second Piola-Kirchhoff stress are coupled via seven different hyperelastic potentials. The Kirchhoff-St.Venant law is compared to three different augmentations of this classical law and three compressible Neo-Hookean materials. Presentations of different hyperelastic materials can e.g. be found in the excellent textbooks by Curnier [14], Holzapfel [15], and Bonet and Wood [16]. It is well-known that the Kirchhoff-St.Venant law fails in compression. Therefore, this standard choice of hyperelastic potential might be improper, especially for topology optimization where it is an obvious risk that this material model might fail for elements with low densities. It is studied in this work if the optimization can be made more robust and efficient by using any of the other six potentials. The optimization is performed for both external forces and prescribed displacements. Topology optimization of non-linear structures for prescribed displacements can be found in Cho and Jung [17] and in the recent work by Huang and Xie [18].

The SIMP-model suggested by Bendsøe [19] is adopted for the design parametrization of the hyperelastic body. In another early work, the SIMP-model was developed and implemented independently by Zhou and Rozvany [20]. The state problem is treated by minimizing the potential energy. In such manner the prescribed displacements are introduced via the Lagrangian function. The corresponding optimality conditions are then solved by using Newton's method. The Jacobian appearing in this step is also used to define the adjoint equation in the sensitivity analysis of the second objective. This is, however, not needed when the potential energy is maximized because of a property resembling the self-adjointness of linear problems, i.e. the sensitivities can be calculated without the need for an adjoint variable. Both optimization problems are solved by the optimality criteria approach (OC). This is derived by linearizing in intervening exponential variables. In such manner one obtains convex and separable approximating problems which can be solved easily by dual solution methods. This approach is also known as sequential convex programming. In this paper we derive the method by solving the necessary optimality conditions. By taking the intermediate variable to be the reciprocal one, we obtain the convex

linearization approach introduced by Fleury [21] and later developed in the work by Fleury and Braibant [22]. The equivalence between sequential convex programming and OC was discussed recently in Groenwold and Etman [23]. Similar discussions can also be found in the textbooks by Haftka and Gürdal [24], and Christensen and Klarbring [26].

The outline of this paper is as follow: in section 2 we introduce the hyperelastic body and present seven different hyperelastic potentials; in section 3 the state equations are derived by minimizing the potential energy; in section 4 our two structural optimization problems are presented; in section 5 the optimality criteria method is derived; and in section 6 two problem settings are studied. Finally, we give some conclusions in section 7.

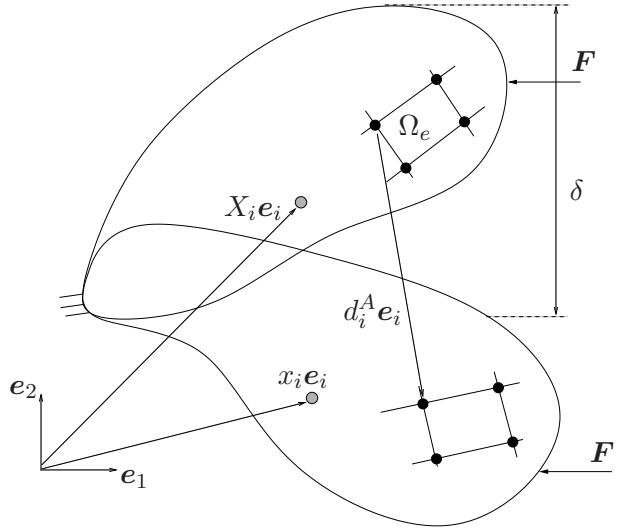

Figure 1: *A hyperelastic body subjected to an external force vector* $\boldsymbol{F}$ *and a prescribed displacement* δ.

2 A hyperelastic body

Let us consider a hyperelastic body, of which a two-dimensional version is given in Figure 1. Position vectors of material points in the reference configuration are denoted $\boldsymbol{X} = X_i \boldsymbol{e}_i$, where $\{\boldsymbol{e}_1, \boldsymbol{e}_2, \boldsymbol{e}_3\}$ is an orthonormal base. When the body deforms these points are mapped to spatial positions $\boldsymbol{x} = \boldsymbol{x}(\boldsymbol{X}) = x_i \boldsymbol{e}_i$. We use a SIMP-interpolation in order to achieve the design parametrization, and the total elastic energy is

written as

$$V = V(\rho_e, E_{ij}) = \sum_{e=1}^{n_{\text{el}}} \rho_e^n \int_{\Omega_e} \Psi(E_{ij})\, \mathrm{d}X_1 X_2 X_3, \tag{3}$$

where n_{el} is the number of finite elements, ρ_e is the design parameter for each element e, n is the SIMP-factor, Ω_e is the reference configuration of element e and $\Psi = \Psi(E_{ij})$ is the hyperelastic strain energy function, which is a function of the Green-Lagrange strain tensor

$$E_{ij} = \frac{1}{2}\left(F_{ki}F_{kj} - \delta_{ij}\right). \tag{4}$$

Here,

$$F_{ij} = \frac{\partial x_i}{\partial X_j} \tag{5}$$

denotes the deformation gradient.

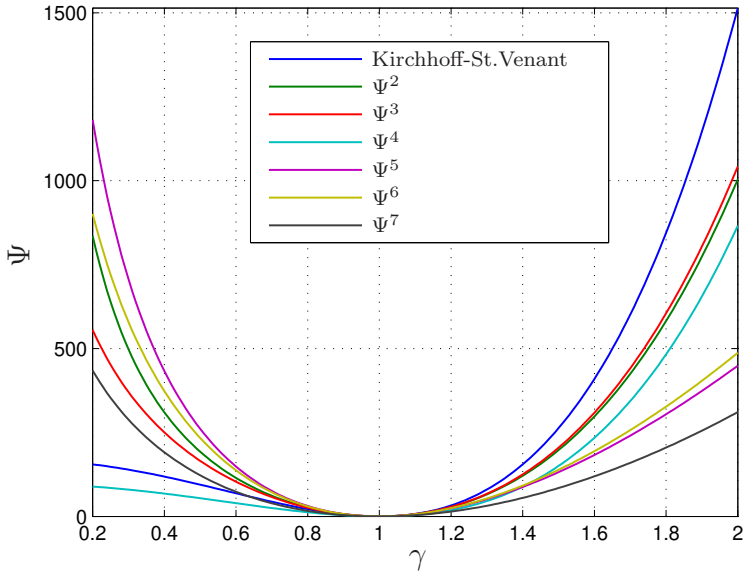

Figure 2: *The strain energy* Ψ *as a function of* γ *(E=1000 units and* μ*=0.3).*

We consider the following explicit functional forms for the strain

energy function Ψ:

$$\Psi^1 = \frac{1}{2}\lambda(E_{kk})^2 + \mu E_{ij}E_{ij}, \tag{6a}$$

$$\Psi^2 = \frac{1}{2}\lambda(\ln J)^2 + \mu E_{ij}E_{ij}, \tag{6b}$$

$$\Psi^3 = \lambda(J - \ln J - 1) + \mu E_{ij}E_{ij}, \tag{6c}$$

$$\Psi^4 = \frac{1}{2}\lambda(J-1)^2 + \mu E_{ij}E_{ij}, \tag{6d}$$

$$\Psi^5 = \frac{1}{2}\lambda(\ln J)^2 + \frac{\mu}{2}(C_{ii} - 3) - \mu \ln J, \tag{6e}$$

$$\Psi^6 = \lambda(J - \ln J - 1) + \frac{\mu}{2}(C_{ii} - 3) - \mu \ln J, \tag{6f}$$

$$\Psi^7 = \frac{1}{2}\lambda(J-1)^2 + \frac{\mu}{2}(C_{ii} - 3) - \mu \ln J. \tag{6g}$$

Here, $J = \det(F_{ij})$, $C_{ij} = 2E_{ij} + \delta_{ij}$ is the right Cauchy-Green deformation tensor, and λ and μ are Lame's material parameters, which are related to Young's modulus E and Poisson's ratio ν via

$$\lambda = \frac{\nu E}{(1+\nu)(1-2\nu)}, \quad \mu = \frac{E}{2(1+\nu)}. \tag{7}$$

The first strain energy Ψ^1 represents the classical Kirchhoff-St.Venant strain energy, and Ψ^2-Ψ^4 are augmentations of Ψ^1 in order to circumvent the well-known draw-backs of the Kirchhoff-St.Venant model obtained in compression at large strains. The final energies Ψ^5-Ψ^7 are compressible Neo-Hookean materials. Ψ^5 and Ψ^7 appear frequently in the literature, while Ψ^6 is a new Neo-Hookean material inspired by the potential Ψ^3 which is a suggestion by Curnier [14]. For the homogenous uniaxial deformation $x_1 = \gamma X_1$, $x_2 = X_2$ and $x_3 = X_3$ ($\gamma > 0$), the corresponding strain energies Ψ^i as a function of γ are plotted in Figure 2.

The second Piola-Kirchhoff stress S_{ij} is defined by

$$S_{ij} = \frac{\partial \Psi}{\partial E_{ij}} \tag{8}$$

and such stresses corresponding to the strain energies in (6) become

$$S^1_{ij} = \lambda E_{kk}\delta_{ij} + 2\mu E_{ij}, \tag{9a}$$
$$S^2_{ij} = \lambda \ln(J) C^{-1}_{ij} + 2\mu E_{ij}, \tag{9b}$$
$$S^3_{ij} = \lambda (J-1) C^{-1}_{ij} + 2\mu E_{ij}, \tag{9c}$$
$$S^4_{ij} = \lambda (J-1) J C^{-1}_{ij} + 2\mu E_{ij}, \tag{9d}$$
$$S^5_{ij} = \lambda \ln(J) C^{-1}_{ij} + \mu(\delta_{ij} - C^{-1}_{ij}), \tag{9e}$$
$$S^6_{ij} = \lambda (J-1) C^{-1}_{ij} + \mu(\delta_{ij} - C^{-1}_{ij}), \tag{9f}$$
$$S^7_{ij} = \lambda (J-1) J C^{-1}_{ij} + \mu(\delta_{ij} - C^{-1}_{ij}). \tag{9g}$$

In the derivation of the stresses above, the following relationship has been utilized:

$$\frac{\partial J}{\partial E_{ij}} = J C^{-1}_{ij}. \tag{10}$$

The Cauchy stress σ_{ij} is given by

$$\sigma_{ij} = \frac{1}{\det(F_{mn})} F_{ik} S_{kl} F_{jl}. \tag{11}$$

For the homogenous uniaxial deformation defined previously, the uniaxial Cauchy stresses σ^i_{11} as a function of γ are plotted in Figure 3. The plots clearly show that the stiffness $k_\sigma = \partial\sigma/\partial\gamma$ has the same value for all models at $\gamma=1$. Furthermore, the softening behavior for the Kirchhoff-St.Venant model in compression is also depicted clearly ($\sigma^1_{11} = 0$ when $\gamma \to 0$, $k^1_\sigma = 0$ when $\gamma = \sqrt{1/3}$), see also Figure 4.

For later use in the development of the Newton method, we also derive explicit expressions for the material elasticity tensor

$$\mathcal{C}_{ijkl} = \frac{\partial^2 \Psi}{\partial E_{ij} \partial E_{kl}}. \tag{12}$$

This results in the following expressions:

$$\mathcal{C}^1_{ijkl} = \lambda \delta_{ij}\delta_{kl} + \mu(\delta_{ik}\delta_{jl} + \delta_{il}\delta_{jk}), \tag{13a}$$
$$\mathcal{C}^2_{ijkl} = \lambda C^{-1}_{ij} C^{-1}_{kl} - \lambda \ln(J) \mathcal{D}_{ijkl} + \mu(\delta_{ik}\delta_{jl} + \delta_{il}\delta_{jk}), \tag{13b}$$
$$\mathcal{C}^3_{ijkl} = \lambda J C^{-1}_{ij} C^{-1}_{kl} - \lambda (J-1) \mathcal{D}_{ijkl} + \mu(\delta_{ik}\delta_{jl} + \delta_{il}\delta_{jk}), \tag{13c}$$
$$\mathcal{C}^4_{ijkl} = \lambda (2J-1) J C^{-1}_{ij} C^{-1}_{kl} - \lambda (J-1) J \mathcal{D}_{ijkl} + \mu(\delta_{ik}\delta_{jl} + \delta_{il}\delta_{jk}), \tag{13d}$$
$$\mathcal{C}^5_{ijkl} = \lambda C^{-1}_{ij} C^{-1}_{kl} - \lambda \ln(J) \mathcal{D}_{ijkl} + \mu \mathcal{D}_{ijkl}, \tag{13e}$$
$$\mathcal{C}^6_{ijkl} = \lambda J C^{-1}_{ij} C^{-1}_{kl} - \lambda (J-1) \mathcal{D}_{ijkl} + \mu \mathcal{D}_{ijkl}, \tag{13f}$$
$$\mathcal{C}^7_{ijkl} = \lambda (2J-1) J C^{-1}_{ij} C^{-1}_{kl} - \lambda (J-1) J \mathcal{D}_{ijkl} + \mu \mathcal{D}_{ijkl}. \tag{13g}$$

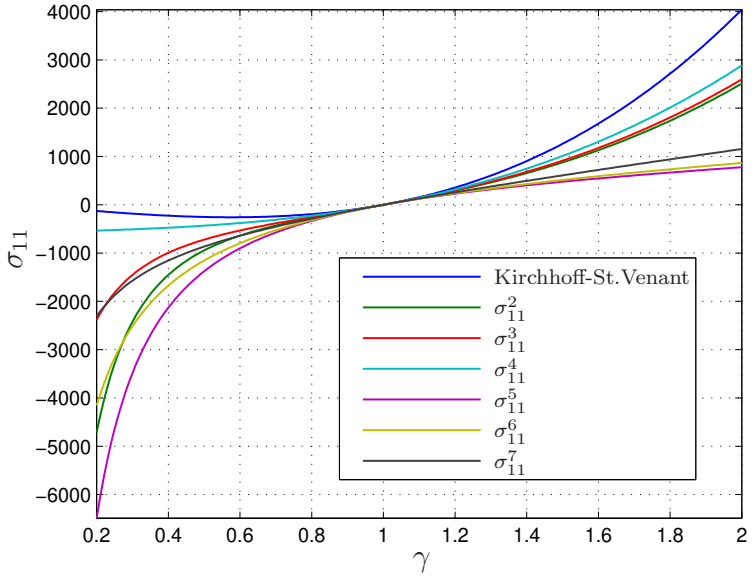

Figure 3: *The uniaxial Cauchy stress σ_{11} as a function of γ.*

Here,

$$\mathcal{D}_{ijkl} = -\frac{\partial C_{ij}^{-1}}{\partial E_{kl}} = \left(C_{ik}^{-1}C_{jl}^{-1} + C_{il}^{-1}C_{jk}^{-1}\right) \tag{14}$$

has been introduced. At $\boldsymbol{x} = \boldsymbol{X}$, we have that $F_{ij} = \delta_{ij}$, $C_{ij} = \delta_{ij}$, $C_{ij}^{-1} = \delta_{ij}$ and $J = 1$. If this is inserted in (13), then all of the elasticity tensors take the form of (13a). The corresponding stiffness coefficients k_σ^i for the uniaxial deformation are plotted in Figure 4.

3 The state problem

A total Lagrangian formulation is adopted, i.e. the kinematics is approximated according to

$$x_i = X_i + N^A d_i^A, \tag{15}$$

where $N^A = N^A(\boldsymbol{X})$ are the finite element interpolation functions and d_i^A are the nodal displacements that are collected in the vector $\boldsymbol{d}$. In a similar way we collect all densities ρ_e in a vector $\boldsymbol{\rho}$.

By inserting (15) into (4), the Green-Lagrange strain tensor becomes

$$E_{ij} = E_{ij}(\boldsymbol{d}) = \frac{1}{2}\left(\frac{\partial N^A}{\partial X_j}d_i^A + \frac{\partial N^A}{\partial X_i}d_j^A + \frac{\partial N^A}{\partial X_i}\frac{\partial N^B}{\partial X_j}d_k^A d_k^B\right). \tag{16}$$

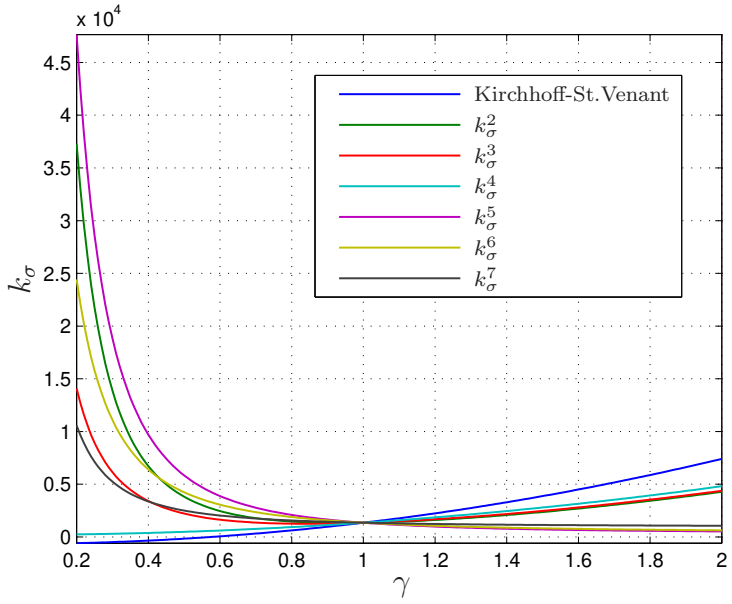

Figure 4: *The stiffness k_σ as a function of γ.*

Taking the derivative of (16) with respect to d_i^A results in

$$\frac{\partial E_{ij}}{\partial d_k^A} = \frac{\partial N^A}{\partial X_j}\left(\delta_{ik} + \frac{\partial N^B}{\partial X_i} d_k^B\right). \tag{17}$$

This gradient will be useful below when the consistent stiffness matrix is derived, see (25).

For a given density distribution $\boldsymbol{\rho} = \hat{\boldsymbol{\rho}}$, our state problem is defined by minimizing the potential energy

$$\Pi = \Pi(\boldsymbol{d}) = V\left(\hat{\boldsymbol{\rho}}, E_{ij}(\boldsymbol{d})\right) - \boldsymbol{F}^T\boldsymbol{d} \tag{18}$$

under satisfaction of the kinematic constraint imposed by the prescribed displacement δ, i.e.

$$\boxed{\begin{cases} \min\limits_{\boldsymbol{d}} \Pi(\boldsymbol{d}) \\ \text{s.t. } \delta - \boldsymbol{e}^T\boldsymbol{d} = 0 \end{cases}} \tag{19}$$

where $\boldsymbol{e}$ is a unit vector representing the direction of the prescribed displacement δ, and $\boldsymbol{F}$ represents the external forces, see Figure 1. The corresponding Lagrangian function is

$$\mathcal{L} = \mathcal{L}(\boldsymbol{\rho}, \boldsymbol{d}, \lambda) = V\left(\boldsymbol{\rho}, E_{ij}(\boldsymbol{d})\right) - \boldsymbol{F}^T\boldsymbol{d} + \lambda(\delta - \boldsymbol{e}^T\boldsymbol{d}), \tag{20}$$

when $\boldsymbol{\rho}$ is taken to be constant. Here, λ is the Lagrange multiplier, which will be identified in (21) as the reaction force required to satisfy $\delta - \boldsymbol{e}^T\boldsymbol{d} = 0$.

The necessary optimality conditions of the problem in Box (19) read

$$\boldsymbol{h} = \boldsymbol{h}(\boldsymbol{d}, \lambda) = \left\{ \begin{array}{c} \dfrac{\partial V}{\partial \boldsymbol{d}} - \boldsymbol{F} - \lambda \boldsymbol{e} \\ \delta - \boldsymbol{e}^T \boldsymbol{d} \end{array} \right\} = \boldsymbol{0}. \tag{21}$$

Here,

$$\boldsymbol{f} = \boldsymbol{f}(\boldsymbol{\rho}, \boldsymbol{d}) = \frac{\partial V}{\partial \boldsymbol{d}} \tag{22}$$

represents the internal elastic forces. A typical member of $\boldsymbol{f}$ is obtained by the following assembly procedure:

$$f_i^A = \bigcap_{e=1}^{n_{\text{el}}} \rho_e^n \int_{\Omega_e} \frac{\partial N^A}{\partial X_k} \left(\delta_{ij} + \frac{\partial N^B}{\partial X_j} d_i^B \right) S_{jk} \, \mathrm{d}X_1 \mathrm{d}X_2 \mathrm{d}X_3, \tag{23}$$

where $\bigcap$ represents the assembly operator.

By taking the derivative of $\boldsymbol{f}$ with respect to $\boldsymbol{d}$ yields the consistent stiffness matrix

$$\boldsymbol{K} = \boldsymbol{K}(\boldsymbol{\rho}, \boldsymbol{d}) = \frac{\partial f}{\partial \boldsymbol{d}} = \frac{\partial^2 V}{\partial \boldsymbol{d}^2}. \tag{24}$$

A typical member of $\boldsymbol{K}$ can be written as

$$\begin{aligned} K_{iq}^{AC} = \frac{\partial f_i^A}{\partial d_q^C} = \bigcap_{e=1}^{n_{\text{el}}} \rho_e^n \int_{\Omega_0} \frac{\partial N^A}{\partial X_k} \frac{\partial N^C}{\partial X_j} \delta_{iq} S_{jk} + \ldots \\ \frac{\partial N^A}{\partial X_k} \left(\delta_{ij} + \frac{\partial N^B}{\partial X_j} d_i^B \right) \mathcal{C}_{jkmn} \frac{\partial E_{mn}}{\partial d_q^C} \, \mathrm{d}X_1 \mathrm{d}X_2 \mathrm{d}X_3. \end{aligned} \tag{25}$$

The equation system in (21) is solved by using Newton's method with an inexact line-search. The Jacobian used for determining the search direction is

$$\boldsymbol{J} = \left[\begin{array}{cc} \dfrac{\partial \boldsymbol{h}}{\partial \boldsymbol{d}} & \dfrac{\partial \boldsymbol{h}}{\partial \lambda} \end{array} \right] = \left[\begin{array}{cc} \boldsymbol{K}(\hat{\boldsymbol{\rho}}, \boldsymbol{d}) & -\boldsymbol{e} \\ -\boldsymbol{e}^T & 0 \end{array} \right]. \tag{26}$$

This Jacobian is also used in the sensitivity analysis of the compliance, see equation (33).

4 The optimization problems

Two different objectives are studied in this work. We will maximize the Lagrangian[1] in (20), and minimize/maximize the compliance of the

[1]For the nested formulation, the last term disappears and the Lagrangian becomes the potential energy.

external forces and the prescribed displacement. Thus, letting $\boldsymbol{d}=\boldsymbol{d}(\boldsymbol{\rho})$ and $\lambda=\lambda(\boldsymbol{\rho})$ be defined implicitly by (19), our two objectives read

$$c^1 = c^1(\boldsymbol{\rho}) = -\mathcal{L}(\boldsymbol{\rho}, \boldsymbol{d}(\boldsymbol{\rho}), \lambda(\boldsymbol{\rho})), \tag{27a}$$

$$c^2 = c^2(\boldsymbol{\rho}) = \frac{1}{2}\boldsymbol{F}^T\boldsymbol{d}(\boldsymbol{\rho}) - \frac{1}{2}\lambda(\boldsymbol{\rho})\delta. \tag{27b}$$

In the case of linear elasticity these two objectives are equivalent. However, this is not true when non-linear elasticity is considered.

Thus, we consider the following nested optimization problems:

$$\boxed{\begin{cases} \min\limits_{\boldsymbol{\rho}} c^i(\boldsymbol{\rho}) \\ \text{s.t.} \begin{cases} V_{\text{vol}}(\boldsymbol{\rho}) \leq \hat{V}_{\text{vol}} \\ \boldsymbol{\epsilon} \leq \boldsymbol{\rho} \leq \mathbf{1} \end{cases} \end{cases}} \tag{28}$$

Here, we have introduced

$$V_{\text{vol}}(\boldsymbol{\rho}) = \sum_{e=1}^{n_{\text{el}}} V_e\rho_e, \qquad V_e = \int_{\Omega_e} \mathrm{d}X_1\mathrm{d}X_2\mathrm{d}X_3, \tag{29}$$

which we constrain by $\hat{V}_{\text{vol}}$. Furthermore, singular design domains are prevented by representing zero element densities by $\boldsymbol{\epsilon}=\{\epsilon,\ldots,\epsilon\}^T$, where $\epsilon > 0$ is a small number, and $\mathbf{1}=\{1,\ldots,1\}^T$.

A nice feature of the first objective is that the sensitivities

$$s_e^1 = \frac{\partial c^1}{\partial \rho_e} = \frac{\partial \mathcal{L}}{\partial \rho_e} + \left(\frac{\partial \mathcal{L}}{\partial \boldsymbol{d}}\right)^T \frac{\partial \boldsymbol{d}}{\partial \rho_e} + \frac{\partial \mathcal{L}}{\partial \lambda}\frac{\partial \lambda}{\partial \rho_e} \tag{30}$$

are easily evaluated without introducing any extra adjoint equation. The optimality conditions in (21) imply that the two latter terms of (30) disappear and we obtain

$$s_e^1 = \frac{\partial \mathcal{L}}{\partial \rho_e} = \frac{\partial V}{\partial \rho_e}. \tag{31}$$

Furthermore, by taking the derivative of (3) with respect to ρ_e, one arrives at

$$s_e^1 = n\rho_e^{(n-1)} \int_{\Omega_e} \Psi(E_{ij})\, \mathrm{d}X_1X_2X_3. \tag{32}$$

The sensitivity of the second objective is derived by the adjoint approach. This is done by introducing the following adjoint equation:

$$\boldsymbol{J}\boldsymbol{\gamma} = \frac{1}{2}\begin{pmatrix} \boldsymbol{F} \\ -\delta \end{pmatrix}. \tag{33}$$

The sensitivity is then obtained as

$$s_e^2 = -\boldsymbol{\gamma}^T \frac{\partial \boldsymbol{h}}{\partial \rho_e}, \tag{34}$$

where

$$\frac{\partial \boldsymbol{h}}{\partial \rho_e} = \left\{ \begin{array}{c} n\rho_e^{n-1} \displaystyle\int_{\Omega_e} \frac{\partial N^A}{\partial X_k} \left(\delta_{ij} + \frac{\partial N^B}{\partial X_j} d_i^B \right) S_{jk} \, \mathrm{d}X_1 \mathrm{d}X_2 \mathrm{d}X_3 \\ 0 \end{array} \right\}. \tag{35}$$

Both sensitivities, (32) and (34), are filtered by using Sigmund's approach [25] before these are inserted in the optimality criteria algorithm presented in the next section.

5 The optimality criteria approach

The problem in Box (28) is solved by an optimality criteria method. This is derived by introducing intervening exponential variables and performing the sensitivity analysis using these variables. In such manner, one obtains a separable approximation which can be treated efficiently by solving the necessary optimality conditions. The outline of the method is presented in this section.

We perform the linearization of the objectives c^i in the intervening variables

$$\xi_e = \rho_e^{-\alpha}, \tag{36}$$

which are collected in $\boldsymbol{\xi}$. Sequential convex programming by using this intervening variable was studied by Groenwald and Etman in [23]. $\alpha > 0$ is a parameter which was set to one in the works by Fleury [21], and by Fleury and Braibant [22]. In this work we have found $\alpha = 0.25$ to be an efficient choice, which corresponds to a damping factor of 0.8 in a standard heuristic OC approach, see e.g. [26, 27]. By considering c^i as functions of $\boldsymbol{\xi}$, i.e. $c^i(\boldsymbol{\xi}) = c^i(\boldsymbol{\rho}(\boldsymbol{\xi}))$ where $\boldsymbol{\rho}(\boldsymbol{\xi})$ is defined by (36), the Taylor expansion of c^i at an iterate $\hat{\boldsymbol{\xi}}$ becomes

$$c^i(\boldsymbol{\xi}) \approx c^i(\hat{\boldsymbol{\xi}}) + \left(\frac{\partial c^i}{\partial \boldsymbol{\xi}} \right)^T \left(\boldsymbol{\xi} - \hat{\boldsymbol{\xi}} \right), \tag{37}$$

The components of the gradient $\partial c^i / \partial \boldsymbol{\xi}$ can be expressed as

$$\zeta_e^i = \frac{\partial c^i}{\partial \xi_e} = \frac{\partial c^i}{\partial \rho_e} \left(-\frac{1}{\alpha} \hat{\xi}_e^{-\frac{1}{\alpha}-1} \right) = s_e^i \left(-\frac{1}{\alpha} \hat{\rho}_e^{1+\alpha} \right), \tag{38}$$

where the sensitivities s_e^i were determined in the previous section, see (32) and (34).

By utilizing ζ_e^i, an approximating sub-problem at a given state $(\hat{\boldsymbol{\rho}}, \hat{\boldsymbol{d}} = \boldsymbol{d}(\hat{\boldsymbol{\rho}}), \hat{\lambda} = \lambda(\hat{\boldsymbol{\rho}}))$ becomes

$$\boxed{\begin{cases} \min\limits_{\boldsymbol{\rho}} \sum\limits_{e=1}^{n_{\text{el}}} \zeta_e^i \rho_e^{-\alpha} \\ \text{s.t.} \begin{cases} V_{\text{vol}}(\boldsymbol{\rho}) - \hat{V}_{\text{vol}} = 0 \\ \hat{\boldsymbol{\rho}} + \boldsymbol{\rho}^l \leq \boldsymbol{\rho} \leq \hat{\boldsymbol{\rho}} + \boldsymbol{\rho}^u \end{cases} \end{cases}} \tag{39}$$

Notice that, without lack of generality, the volume constraint is written on equality form instead as an inequality in order to simplify the derivation of the OC algorithm. Here, $\boldsymbol{\rho}^l$ and $\boldsymbol{\rho}^u$ represent lower and upper move limits, respectively.

The corresponding Lagrangian function for each problem (i=1 or 2) in (39) is

$$\mathcal{M}(\boldsymbol{\rho}, \tau) = \sum_{e=1}^{n_{\text{el}}} \zeta_e^i \rho_e^{-\alpha} + \tau(\sum_{e=1}^{n_{\text{el}}} V_e \rho_e - \hat{V}_{\text{vol}}), \tag{40}$$

where τ is a Lagrangian multiplier. For $\hat{\rho}_e + \rho_e^l < \rho_e < \hat{\rho}_e + \rho_e^u$, the corresponding optimality conditions read

$$\frac{\partial \mathcal{M}}{\partial \rho_e} = -\alpha \zeta_e^i \rho_e^{-\alpha-1} + \tau V_e = 0, \tag{41a}$$

$$\frac{\partial \mathcal{M}}{\partial \rho_e} = \sum_{e=1}^{n_{\text{el}}} V_e \rho_e - \hat{V}_{\text{vol}} = 0. \tag{41b}$$

By solving (41a), one gets

$$\rho_e^{\text{sol}} = \rho_e^{\text{sol}}(\tau) = \left(\frac{\alpha \zeta_e^i}{\tau V_e} \right)^{\frac{1}{1+\alpha}}. \tag{42}$$

This solution must of course also be checked such that $\hat{\rho}_e + \rho_e^l \leq \rho_e \leq \hat{\rho}_e + \rho_e^u$ is satisfied. Otherwise, the solution is taken to be the lower or the upper limit, respectively. In conclusion, for given Lagrangian multiplier τ the minimum point of $\mathcal{M}(\boldsymbol{\rho}, \tau)$ is given by

$$\rho_e(\tau) = \begin{cases} \rho_e^l & \text{if } \rho_e^{\text{sol}} < \hat{\rho}_e + \rho_e^l \\ \rho_e^{\text{sol}}(\tau) & \text{if } \hat{\rho}_e + \rho_e^l \leq \rho_e^{\text{sol}} \leq \hat{\rho}_e + \rho_e^u \\ \rho_e^u & \text{if } \rho_e^{\text{sol}} > \hat{\rho}_e + \rho_e^u. \end{cases} \tag{43}$$

The unknown multiplier τ is found by inserting (43) into (41b) and solving the resulting nonlinear equation, e.g. by using Newton's method

as done in this work. At an iterate τ^k, the search direction is then given by

$$s = -\frac{h(\tau^k)}{h'(\tau^k)}, \tag{44}$$

where

$$h(\tau) = \sum_{e=1}^{n_{\text{el}}} V_e \rho_e(\tau) - \hat{V}_{\text{vol}} = 0 \tag{45}$$

and

$$h'(\tau) = \sum_{e=1}^{n_{\text{el}}} \begin{cases} 0 & \text{if } \rho_e^{\text{sol}} < \hat{\rho}_e + \rho_e^l \\ -\dfrac{V_e}{1+\alpha} \left(\dfrac{\alpha \zeta_e^i}{V_e} \right)^{\frac{1}{1+\alpha}} \left(\dfrac{1}{\tau} \right)^{\frac{2+\alpha}{1+\alpha}} & \text{if } \hat{\rho}_e + \rho_e^l \leq \rho_e^{\text{sol}} \leq \hat{\rho}_e + \rho_e^u \\ 0 & \text{if } \rho_e^{\text{sol}} > \hat{\rho}_e + \rho_e^u. \end{cases} \tag{46}$$

When a solution $\hat{\tau}$ is found the next iteration point, where a new subproblem such as (39) is formulated, is given by equation (43) as $\rho_e(\hat{\tau})$.

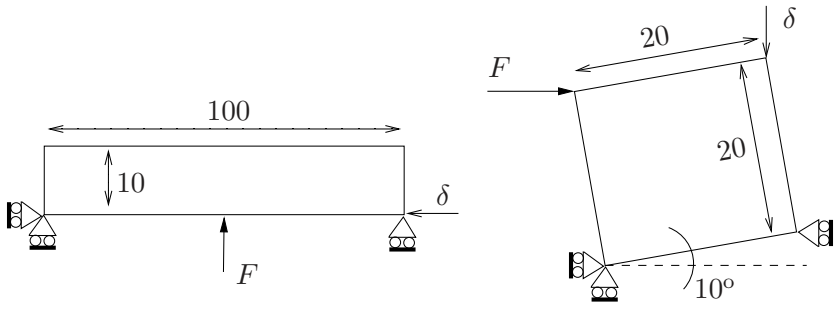

Figure 5: *Two problem settings. All dimensions are given in [mm].*

6 Numerical examples

The two general problem settings presented in Figure 5 are studied for both of our presented optimization problems and the seven hyperelastic material models as well as linear elasticity. Thus, 16 different combinations of objective and elasticity model for each problem setting are solved and evaluated. Since the second problem is solved for two differen values of the prescribed displacement, 48 optimization problems are considered in this section. The theory presented in the previous sections is implemented by using Matlab and Intel Fortran, where the

Fortran code is linked to Matlab as mex-files. The problems are solved using this implementation on a laptop with an Intel Core i7 2.67 GHz processor. The linear equation systems are solved by using the sparse Cholesky solver of Matlab.

The first problem setting concerns a beam with dimensions 100×10 [mm] and is inspired by study in Niu et al. [1]. The beam is fixed vertically at the right end and it is fixed in both directions at the other end. An external force F is applied at the center and at the right end a displacement δ is prescribed.

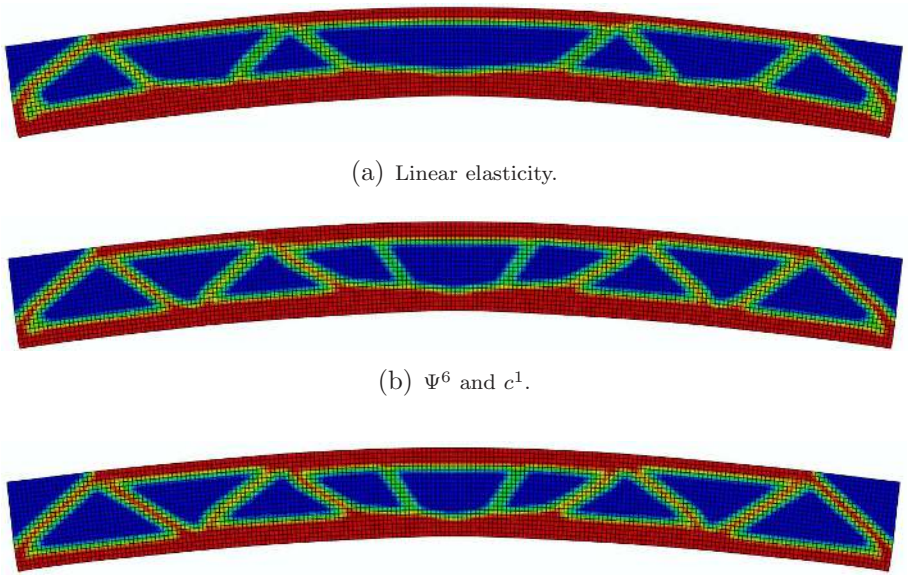

(a) Linear elasticity.

(b) Ψ^6 and c^1.

(c) Ψ^6 and c^2.

Figure 6: *The first problem setting solved for both linear and non-linear elasticity. There is a clear difference between these two cases, while the choice of stiffness objective does not influence the concept.*

The second problem setting concerns a square plate with dimensions 20×20 [mm^2]. The reference configuration of the plate is rotated 10 degrees counter-clockwise. The lower left end is then fixed in both directions, and the lower right end is fixed horizontally. The upper right corner is subjected to a displacement δ vertically and, finally, an external force F is applied horizontally at the upper left corner.

Both structures are modeled by using fully integrated bilinear elements where the plain strain assumption is adopted. Young's modulus and Poison's ratio are set to 21000 [N/mm^2] and 0.3, respectively. The number of elements for the beam is 4000 and for the square plate 6400

elements are used.

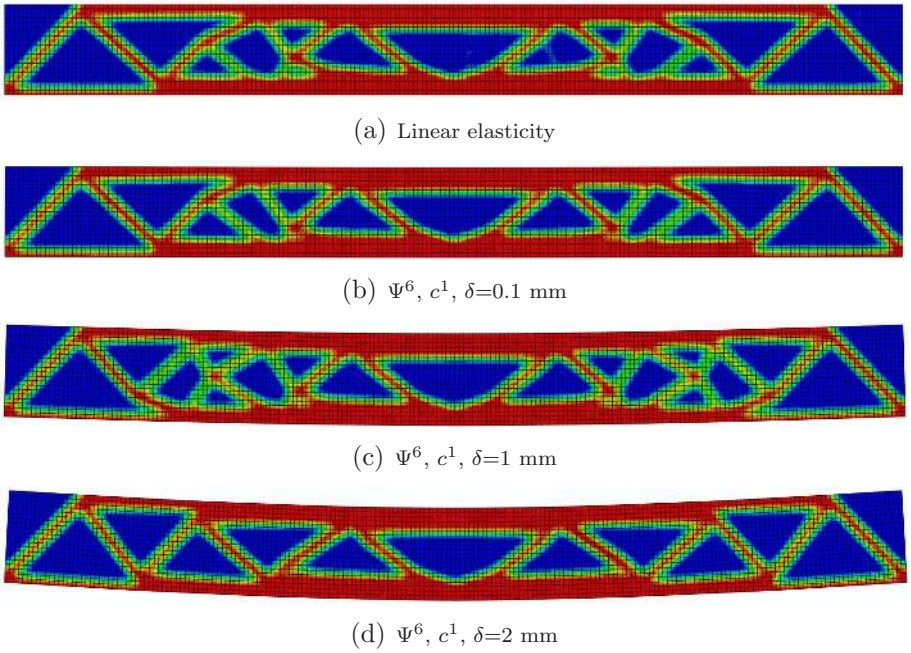

(a) Linear elasticity

(b) Ψ^6, c^1, δ=0.1 mm

(c) Ψ^6, c^1, δ=1 mm

(d) Ψ^6, c^1, δ=2 mm

Figure 7: *The MBB-benchmark solved with linear and non-linear elasticity. The force is represented by a prescribed displacement δ downwards.*

The first problem is studied for a force F=1000 [N] and δ=2 [mm]. The optimal solutions are obtained after 150 OC loops. This number of loops is a conservative choice in order to guarantee convergence in the objectives. The filter radius is 0.8 [mm] and the move limits are set to $\pm$0.0125. The admissible volume of material is constrained by a volume fraction of 50%. The problem is solved for the standard small displacement linear elasticity setting as well as for our large displacement setting using the seven elastic energies Ψ^i. The optimal solutions for the linear case and when Ψ^6 is chosen are plotted in Figure 6. Even if the displacements are moderately large in this particular case, one might assume from an engineering point of view that these are still so small that a small displacement theory is sufficient. However, this is not the case. It is obvious that the linear and non-linear solutions differ. Now, one might assume that the choice of strain energy Ψ^i might influence the solution. However, this is not the case in this problem. Moreover, we obtain very similar solutions for the two different objectives c^i, see Figure 6.

If one neglects the prescribed displacement in the first problem, then the established MBB-benchmark is recovered, see e.g. [26, 27].

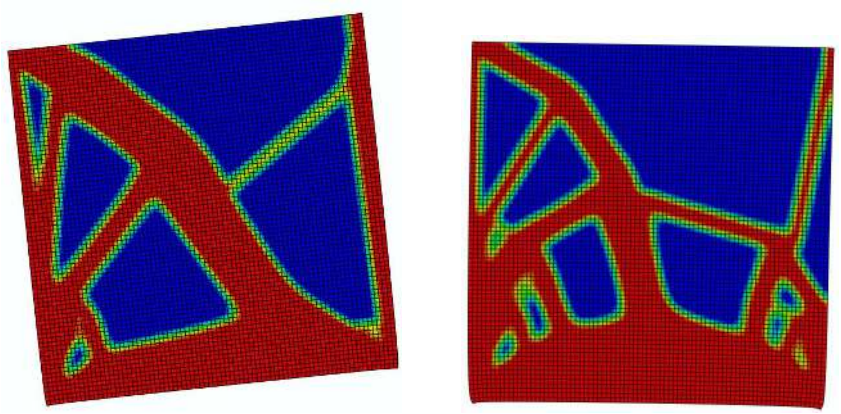

(a) Linear elasticity, δ=1 mm.

(b) Linear elasticity, δ=3 mm.

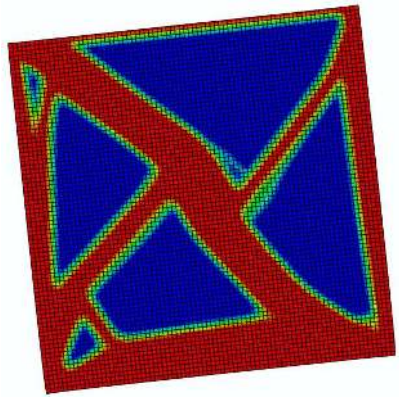

(c) Ψ^6, c^1, δ=1 mm.

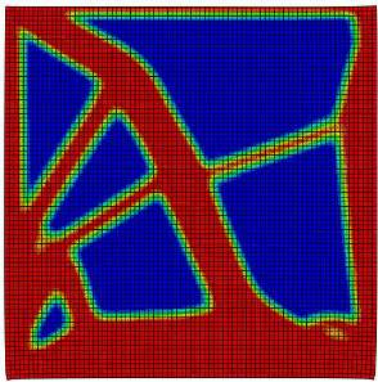

(d) Ψ^6, c^1, δ=3 mm.

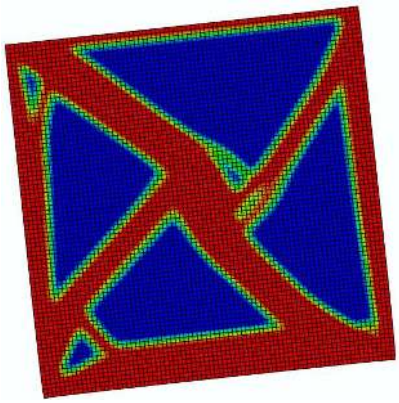

(e) Ψ^6, c^2, δ=1 mm.

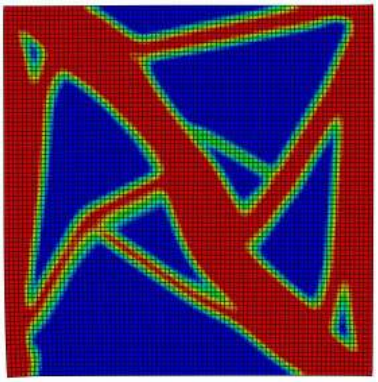

(f) Ψ^6, c^2, δ=3 mm.

Figure 8: *The second problem setting solved for both large and small displacements and different stiffness objectives. The difference between small and large displacement theory is pronounced. When $\delta = 3$ [mm] the difference in solutions for different objectives is also large.*

The differences between the linear and non-linear solutions also appear for this situation. This is shown in Figure 7, where the linear solution is compared to a sequence of non-linear solutions obtained for different magnitudes of the force. The problem is treated by applying a prescribed displacement at the center with different magnitudes downwards. The linear and non-linear solutions begin to diverge already at δ=1 [mm], and for δ=2 [mm] a clear difference in the solutions can be noticed. From an engineering point of view, this displacement might be regarded as small.

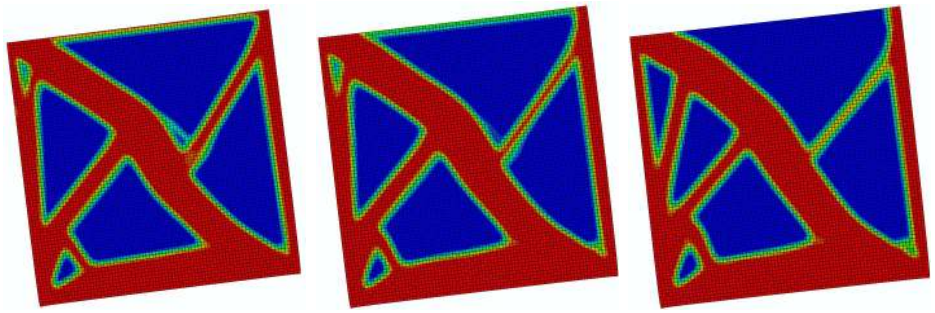

(a) Lin. elast., δ=0.7 mm (b) Lin. elast., δ=0.8 mm (c) Lin. elast., δ=0.9 mm

(d) Ψ^6, c^1, δ=0.7 mm (e) Ψ^6, c^1, δ=0.8 mm (f) Ψ^6, c^1, δ=0.9 mm

Figure 9: *For δ <0.7 [mm], the linear and non-linear models generate the same optimal topology. But for larger displacements the solutions begin to diverge and a clear difference is apparent for δ >1 [mm].*

The second problem is also studied for a constant force F of 1000 [N] but for a varying displacement δ. Initially, the prescribed displacement is taken to be 1 and 3 [mm], respectively. We use again 150 OC loops with move limits equal to $\pm$0.0125. The filter radius is slightly smaller and set to 0.5 [mm]. The admissible volume of material is again constrained by a volume fraction of 50%. The optimal solutions depend on the deformations. This is illustrated in Figure 8, where the optimal solutions for linear elasticity and Ψ_6 are presented. A clear difference is

apparent between the linear case and the non-linear model. One might be surprised that this difference appears in the case of small rotations, i.e. when δ=1 [mm]. This is somewhat in contrast to the statement in [4] where it is concluded that the importance of non-linear modeling in stiffness design is marginal. It is obvious that the box concept generated by the hyperelastic formulation is to prefer over the concept generated by the linear elasticity model. Of course, for sufficiently small displacements, the linear and non-linear models will produce the same solution. In fact, for δ <0.7 [mm], the same solution is generated by the linear and the non-linear models. The divergence in solution begins for δ >0.7 [mm] and clearly appears for δ >1 [mm] (i.e. for rotations less than 3 deg as announced in the abstract). This is shown in Figure 9, where one can see how the stiffener at the top is removed and the box concept is destroyed in the linear case, but remains in the non-linear models. Furthermore, the solutions obtained for different objectives are more or less identical when δ=1 [mm]. However, when δ equals 3 [mm], one obtains different solutions. In our opinion, the box concept generated by maximizing the Lagrangian is to prefer over the concept generated by minimizing/maximizing the compliance. The solutions obtained for the other energies are very similar when δ=1 [mm]. But, when δ=3 [mm], the Kirchhoff-St.Venant model produces a solution which is different from the solutions obtained by the other energies, see Figure 10.

The major difference between different strain energies is obtained in the numerical performance. In general, the convergence of the Kirchhoff-St.Venant model is remarkable slower than the other energies which are very similar in performance. In average 3-5 Newton iterations are needed per OC loop for the problems presented in this section when Ψ^2-Ψ^7 are used. However, this number is doubled for the Kirchhoff-St.Venant model. The CPU-time per OC loop is approximately 3-4 [s] for Ψ^2-Ψ^7 (including the assembly procedure). The bottle-neck of the algorithm is to solve the linear system of equations. Therefore, using c^1 is preferable since no adjoint problem needs to be solved and the CPU-time will be approximately 20% shorter than the time we obtain when using c^2.

The values of the move limits ($\pm$0.0125) are a most conservative choice in order to make all optimizations robust for all possible settings. In particular, we need these conservative limits in order to obtain robustness in the Newton algorithm for solving the state problem. If too large move limits are taken, then the Newton algorithm might fail when the Kirchhoff-St.Venant model is solved. However, for the other hyperelastic materials, these conservative values are typically not needed and we can instead use move limits of $\pm$0.1.

7 Concluding remarks

In this work topology optimization of hyperelastic bodies are studied for seven different elastic potentials by maximizing the potential energy and optimizing the compliance. The following remarks and conclusions can be made:

- Rotations that would typically be regarded as small, and treatable by linear theory in standard stress analysis, **might not** be seen as small in topology optimization: even for such small rotations topologies generated by using a linear state problem may differ from those produced by a non-linear formulation valid for large displacements. In the problems shown in this paper it is only in the limit of very small rotations that the two topologies coincide.

- The choice of stiffness objective is not obvious in optimization based on large deformation theory, and if non-zero prescribed displacements is included it is an issue even for linear elasticity. However, in a recent publication [3], we showed that potential energy is the natural objective that includes both types of loading. In the present paper it becomes clear that for large deformation theory a further reason to choose the potential energy objective (27a), instead of the direct generalization of the classical compliance objective (27b), is that the sensitivity analysis becomes simple: no adjoint equation needs to be solved in the first case, which in large deformations is needed for the second objective. It is also rather obvious, since the two objectives are not mathematically equivalent, that they may in some cases produce different topologies which is shown for the second problem setting in this paper.

- The Kirchhoff-St.Venant model is known to have unphysical behavior in compression but despite this is usually considered to be a reasonable choice in stress analysis including somehow small strains but large displacements. However, we note in this paper that in topology optimization the numerical performance of the Kirchhoff-St.Venant model is always significantly worse than the performance obtained for models including a generally more physical behavior in compression. The reason for this fact could be traced to elements with low densities that are interpreted as void parts of the structure. Note that we do not discuss which of the different strain energy potentials that is somehow the most physically correct in a large deformation problem: in the range of

loadings we are considering they are essentially equivalent. However, in a practical problem involving large strains, this would obviously be an issue.

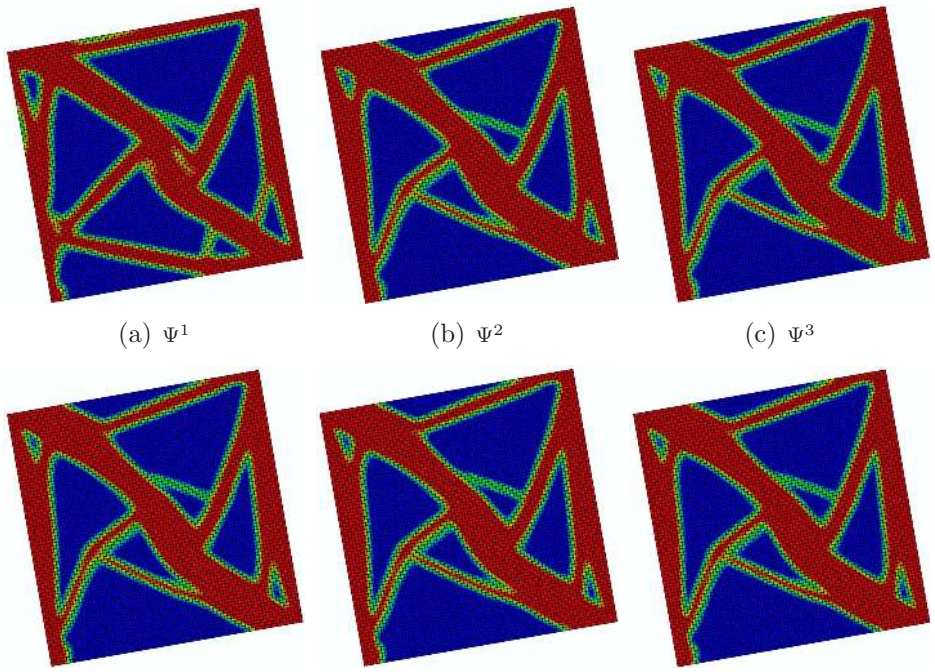

(a) Ψ^1 (b) Ψ^2 (c) Ψ^3

(d) Ψ^4 (e) Ψ^5 (f) Ψ^7

Figure 10: *The second problem setting solved when δ=3 [mm] for Ψ_1 through Ψ_7. Optimal solutions are plotted on the reference configuration. It is clear that the Kirchhoff-St.Venant model gives a different solution compared to the solutions obtained when using the other hyperelastic potentials.*

Acknowledgement *This project was financed by Swedish Foundation for Strategic Research through the ProViking programme.*

References

[1] Niu, F., Xu, S. & Cheng, G., A general formulation of structural topology optimization for maximizing structural stiffness, *Structural and Multidisciplinary Optimization* (2011) **43**:561-572.

[2] Pedersen, P. & Pedersen, N., Design objectives with non-zero prescribed support displacements, *Structural and Multidisciplinary Optimization* (2011) **43**:205–214.

[3] Klarbring, A. & Strömberg, N., A note on the min-max formulation of stiffness optimization including non-zero prescribed displacements, *Structural and Multidisciplinary Optimization* (2011) DOI: 10.1007/s00158-011-0674-3.

[4] Buhl, T., Pedersen, C.B. & Sigmund, O., Stiffness design of geometrically nonlinear structures using topology optimization, *Structural and Multidisciplinary Optimization* (2000) **19**:93–104.

[5] Gea, H.C. & Luo, J., Topology optimization of structures with geometrical nonlinearities, *Computers and Structures* (2001) **79**:1977–1985.

[6] Bruns, T.E. & Tortorelli, D., Topology optimization of non-linear elastic structures and compliant mechanisms, *Computer Methods in Applied Mechanics and Engineering* (2001) **190**:3443–3459.

[7] Pedersen, C., Buhl, T. & Sigmund, O., Topology synthesis of large-displacement compliant mechanisms, *International Journal of Numerical Methods in Engineering* (2001) **50**:2683–2705.

[8] Jung, D. & Gea, H.C., Topology optimization of nonlinear structures, *Finite Elements in Analysis and Design* (2004) **40**:1417–1427.

[9] Bruns, T.E., Sigmund, O. & Tortorelli, D.A., Numerical methods for the topology optimization of structures that exhibit snap-through, *International Journal of Numerical Methods in Engineering* (2002) **55**:1215–1237.

[10] Bruns, T.E. & Sigmund, O., Toward the topology design of mechanisms that exhibit snap-through behavior, *Computer Methods in Applied Mechanical Engineering* (2004) **193**:3973–4000.

[11] Kemmler, R., Lipka, A. & Ramm, E., Large deformations and stability in topology optimization, *Structural and Multidisciplinary Optimization* (2005) **30**:459–476.

[12] Pajot, J.M. & Maute, K., Analytical sensitivity analysis of geometrically nonlinear structures based on the co-rotational finite element method, *Finite Elements in Analysis and Design* (2006) **42**:900–913.

[13] Lee, W.S. & Youn, S.K., Topology optimization of rubber isolators considering static and dynamic behaviours, *Structural and Multidisciplinary Optimization* (2004) **27**:284-294.

[14] Curnier, A., *Computational Methods in Solid Mechanics*, Kluwer Academic Publishers, 1994.

[15] Holzapfel, G.A., *Nonlinear Solid Mechanics, A Continuum Approach for Engineering*, John Wiley and Sons Ltd, 2000.

[16] Bonet, J. & Wood, R.D., *Nonlinear Continuum Mechanics for Finite Element Analysis*, Cambridge University Press, 2008.

[17] Cho, S. & Jung, H-S., Design sensitivity analysis and topology optimization of displacement-loaded non-linear structures, *Computer Methods in Applied Mechanical Engineering* (2003) **192**:2539–2553.

[18] Huang, X. & Xie, Y.M., Topology optimization of nonlinear structures under displacement loading, *Engineering Structures* (2008) **30**:2057–2068.

[19] Bendsøe, M.P. Optimal shape design as a material distribution problem, *Structural Optimization* (1989) **1**:193-202.

[20] Zhou, M. & Rozvany, G.I.N., The COC algorithm, part II: Topological, geometrical and generalized shape optimization, *Computer Methods in Applied Mechanics and Engineering* (1991) **89**:309-336.

[21] Fleury, C., Structural weight optimization by dual methods of convex programming, *International Journal for Numerical Methods in Engineering* (1979) **14**:1761–1783.

[22] Fleury, C. & Braibant, V., Structural optimization: a new dual method using mixed variables, *International Journal for Numerical Methods in Engineering* (1986) **23**:409–428.

[23] Groenwold, A.A. & Etman, L.F.P., On the equivalence of optimality criterion and sequential approximate optimization methods in the classical topology layout problem, *International Journal for Numerical Methods in Engineering* (2008) **73**:297–316.

[24] Haftka, R.T. & Gürdal, Z., *Elements of Structural Optimization*, Kluwer Academic Publishers, 1992.

[25] Sigmund, O., A 99 line topology optimization code written in Matlab, *Structural and Multidisciplinary Optimization* (2001), **21**:120-127.

[26] Christensen, P. & Klarbring, A., *An Introduction to Structural Optimization*, Springer, 2008.

[27] Bendsøe, M. & Sigmund, O., *Topology Optimization, Theory, Methods and Applications*, Springer, 2002.